Contents lists available at ScienceDirect

Marine and Petroleum Geology

journal homepage: www.elsevier.com

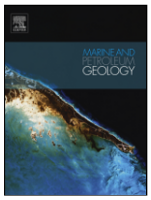

Research paper

Comparing optical and Raman spectroscopic investigations of phytoclasts and sporomorphs for thermal maturity assessment: The case study of Hettangian continental facies in the Holy cross Mts. (central Poland)

A. Schito [a, *], A. Spina [b], S. Corrado [a], S. Cirilli [b], C. Romano [a]

[a] Università degli Studi di Roma Tre, Dipartimento di Scienze, Sezione di Scienze Geologiche, Largo San Leonardo Murialdo 1, 00146, Rome, Italy
[b] Università degli Studi di Perugia, Dipartimento di Fisica e Geologia, Via Alessandro Pascoli, 06123, Perugia, PG, Italy

ARTICLE INFO

Keywords:
Thermal maturity
Raman spectroscopy
Palynomorph Darkness Index
Multivariate data analysis

ABSTRACT

Thermal maturity of six organic rich samples from Jurassic continental successions cropping out in the Holy Cross Mountains in Central Poland, has been characterized by classic thermal maturity indicators, micro-Raman spectroscopy and Palynomorph Darkness Index, in order to create a multi-method workflow for complex palynofacies thermal maturity assessment. Transmitted light observations on dispersed organic matter define a Hettangian lacustrine depositional environment, characterized by periods of reducing/oxidizing conditions and variable sedimentation rates. Thermal maturity detected by classical maturity indicators and PDI indicates an early maturation stage of hydrocarbon generation and is in agreement with spectroscopic analyses performed on phytoclast groups. Moreover, Raman parameters in the sporomorph group indicate a systematic shift toward a lower degree of aromatization compared to the phytoclast group. Finally, the multivariate statistical analysis performed on Raman spectra is found to be a promising tool to define and predict the heterogeneity of dispersed organic matter in sediments.

1. Introduction

Palynofacies analyses of organic matter dispersed in sediments under transmitted light observations, have been often coupled with reflectance analyses in order to constrain the thermal maturation of sedimentary successions. Vitrinite reflectance is generally the most used and commonly accepted thermal maturity indicator. However, the absence/scarcity of vitrinite and/or the suppression/retardation of its reflectance could produce high uncertainties especially in Lower Paleozoic and oil-prone source rocks (Caricchi et al., 2016; Schito et al., 2018). In this case, other optical methods could represent a viable alternative to establish the thermal maturity of organic matter. These are mainly based on the capability of palynomorph wall color to evolve progressively in response to increasing temperature. Color alteration can be measured by the Thermal Alteration Index (TAI; Staplin, 1969), the Spore Color Index (SCI; Smith, 1983) or the Acritarch Alteration Index (AAI; Legall et al., 1981; Williams et al., 1998). All these indicators are based on visual inspection of a selected class of palynomorphs, and therefor they are only qualitative in nature and strongly dependent on the operator. As an alternative, Goodhue and Clayton (2010) proposed a new semi-quantitative method for the assessment of dispersed organic matter maturation, based on simple digital images analysis (Palynomorph Darkness Index -PDI).

Changes in color alteration, as well as changes in vitrinite reflectance with increasing thermal maturity reflect chemical and structural modifications in the molecular structure of the organic matter. In fact, at the same maturity rank, palynomorphs and phytoclasts have different C/H and C/O ratios (Espitalié et al., 1987; Behar et al., 1992) and degree of “aliphaticity” and “aromaticity” (Ganz et al., 1990; Ibarra et al., 1996; Lis et al., 2005; Chen et al., 2012). Only few studies have investigated the differences between palynomorphs and phytoclasts by means of FT-IR spectroscopy and Raman spectroscopy (Yule et al., 2000; Marshall et al., 2005).

Raman spectroscopy, in particular, has shown to be a promising tool to study the structural order of carbonaceous material in metamorphism (Beyssac et al., 2002; Lahfid et al., 2010; Ferralis et al., 2016; Lünsdorf et al., 2017), but only recently its application has been extended in to the diagenetic realm (Liu et al., 2013; Hinrichs et al.,

* Corresponding author.
Email address: andrea.schito@uniroma3.it (A. Schito)

https://doi.org/10.1016/j.marpetgeo.2019.03.008
Received 25 September 2018; Received in revised form 6 March 2019; Accepted 8 March 2019
Available online xxx

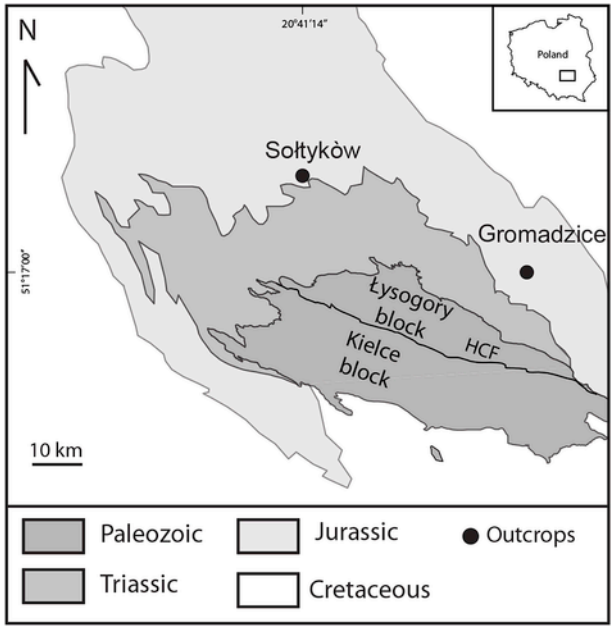

Fig. 1. Simplified sketch map of the Holy Cross Mountains area showing sampling and outcrops location. Acronyms: HCF = Holy Cross Fault. Black dots refer to sampling outcrops location. Redrawn after Schito et al. (2017b).

2014; Schito et al., 2017a; Schmidt et al., 2017; Hackley and Lunsdorf, 2018; Khatibi et al., 2018; Schito and Corrado, 2018). In this study, we focus on the differences in the Raman signal between phytoclasts and sporomorphs on a set of six organic rich samples at the same maturation stage, corresponding to the onset of the oil window.

To reach this aim, thermal maturity was first assessed by means of both reflected and transmitted light analyses, then compared with Raman parameters carried out from an automatic deconvolution (Schito and Corrado, 2018).

2. Geological setting

The Holy Cross Mountains (HCM) are located in south-central Poland (Dadlez, 2001) to the West of the Trans European Suture Zone, a tectonic boundary between the eastern and western European Platform (Belka, 1990). In this area, Cambrian to Carboniferous sedimentary successions crop out beneath a Permian to Cretaceous cover of continental to marine successions.

The HCM are composed of the Kielce block (portion of the Małopolska block) to the South and the Łysogory block to the North, separated by a deep-seated regional fault, known as the Holy Cross Fault (Fig. 1, Lamarche et al., 1999; Konon, 2007). Paleozoic successions of the two blocks comprise different lithologies from shallow water carbonates to basinal shales, marls and limestones (Szulczewski et al., 1996; Belka and Narkiewicz, 2008; Kozłowski et al., 2014) and were affected by different orogenic cycles that led to exhumation of the area at the end of the Variscan cycle (Lamarche et al., 1999; Konon, 2004, 2007).

Since Permian times the area was part of the Mid-Polish Thought (Dadlez et al., 1994) and the Paleozoic successions were unconformably covered by an upper Permian-Lower Triassic continental-clastic deposits (Kutek and Głazek, 1972; Dadlez et al., 1994; Hakenberg and Świdrowska, 1997). The transition between Upper Triassic and Lower Jurassic sedimentation was marked by a net climate transition from arid to more humid conditions (Pienkowski, 2004). Lower Jurassic deposits lie in unconformity on the Upper Triassic and consist of alluvial, lacustrine and deltaic deposits covered by near-shore and marine sediments (Pienkowski, 2004; Marynowski and Simoneit, 2009).

3. Materials

We analysed a Hettangian succession cropping out in the Sołtykow and Gromadzice localities (Fig. 1). Five samples were collected from arenitic and shaly horizons in Lower Jurassic lacustrine facies at the base of the Zagaje Formation cropping out at Sołtykow locality (samples HCM 17.1, 17.2, 17.3, 17.4, 17.5; Pienkowski, 2004; Pienkowski and Waksmundzka, 2009). Another sample was collected from a shaly horizon in the Skłoby Formation (Gromadzice outcrop, HCM 18.1 sample).

Total organic carbon (TOC) ranges from 0.87 to 5.89 wt%, whereas Tmax values derived from Rock-Eval Pyrolysis range between 433 and 439 °C (Schito et al., 2017b and Table 1) indicating an immature to early mature stage with respect to hydrocarbon generation. Samples for vitrinite reflectance analyses were first crushed in an agate mortar, then mounted on epoxy resin and polished according to Robl and Davis' method (1993). For PDI and micro-Raman analyses, organic matter was concentrated from five samples (17.2, 17.3, 17.4, 17.5, 18.1) by acid maceration (HCl 37% and HF 50%) and filtration of the organic-rich residue at 10 mm.

For palynological analysis samples were processed using a combination of standard palynological techniques (Heusser and Stock, 1984; Wood et al., 2002; Batten and Stead, 2005; Traverse, 2007). Twenty grams of sediments from each sample were dissolved in 37% HCl and 50% HF to isolate the organic fraction and, after neutralization, sieved at 10 μm. No oxidation was performed on the organic residue. A minimum of two palynological strew-slides were mounted for each sample using Eukitt as a mounting medium. Palynological slides were examined using a transmitted-light Leica DM1000 microscope, commonly with × 20 (dry) and × 100 (oil immersion) objectives.

4. Methods

4.1. Optical analyses

Samples for vitrinite reflectance analyses were analysed in reflected, non-polarized, monochromatic light ($\lambda = 546$ nm) under oil immersion ($\nu = 1.518$) using a Zeiss Axioskop MPM400 microscope equipped with MPS 200 system by J&M Analytik AG. The standard materials used to calibrate the microscope are a Spinel with relative reflectance of 0.426% (R_r), Saphir with R_r of 0.585% and YAG (Yttrium-Alluminium-Garnet) with R_r of 0.905%. About 50 measurements for each sample were taken in order to statistically constrain heterogeneities in the analysed kerogen.

In Palynological analysis, the organic particles were classified according to their origin, taking into account the available classification schemes (e.g., Whitaker, 1984; Van der Zwan, 1990; Steffen and Gorin, 1993a,b; Tyson, 1995; Batten, 1996; Batten and Stead, 2005). Three-hundred particles per slide (two slides for each sample) have been counted in order to estimate the relative percentages of the organic constituents. The samples were processed and the palynological slides were stored at the Sedimentary Organic Matter Laboratory of the Department of Physics and Geology, University of Perugia (Italy).

Optical microscope methods such as TAI (Staplin, 1969) and SCI (Collins, 1990; Fisher et al., 1980; Haseldonckx, 1979; Hillier and Marshall, 1992; Marshall and Yule, 1999; Pearson, 1990) were also utilized in this study to assess the thermal maturity of organic matter. TAI and SCI were established from the color of smooth, unfolded and unornamented sporomorph specimens as *Calamospora* sp., *Deltoidospora* sp. and *Retusotriletes* sp. based on a visual comparison to Munsell color standards (Pearson, 1990 in Traverse, 2007). TAI and SCI methods use a five and ten point scale, respectively. Both reflect a color gradation

Table 1
Organic parameters, PDI, SCI, TAI, Ro and Rock-Eval Pyrolysis values. Rock-Eval Pyrolysis from Schito et al. (2017b).

Samples	POF(%)	MOF(%)	BOF (%)	SG (%)	AP (%)	AE (%)	PDI (%)	TAI	SCI	Ro (%)	Rotot (%)	RoeqPDI (%)	TOC (wt%)	S1 (mg/g)	S2 (mg/g)	HI (mg/g)	Tmax (°C)
HCM 18.1	34%	22%	35%	6%	2%	1%	47	2.3	4.5	0.46 ± 0.04	0.53 ± 0.13	0.54	5.89	0.04	2.25	38	433
HCM 17.5	18%	21%	16%	27%	13%	5%	42	2.6	6.5	0.49 ± 0.05	–	0.46	1.66	0.02	2.87	173	437
HCM 17.4	13%	31%	13%	30%	8%	5%	41	2.4	5	0.49 ± 0.05	–	0.45	1.33	0.01	2.36	177	438
HCM 17.3	23%	35%	20%	15%	7%	0%	46	2.5	5.5	0.47 ± 0.05	–	0.53	0.87	0.01	0.52	60	439
HCM 17.2	22%	27%	15%	33%	3%	0%	46	2.4	5	0.46 ± 0.05	0.53 ± 0.12	0.53	4.72	0.01	1.5	32	439
HCM 17.1	34%	12%	38%	10%	6%	0%	N.D.	N.D.	N.D.	0.51 ± 0.03	–	N.D.	0.39	0.01	0.13	33	N.D.

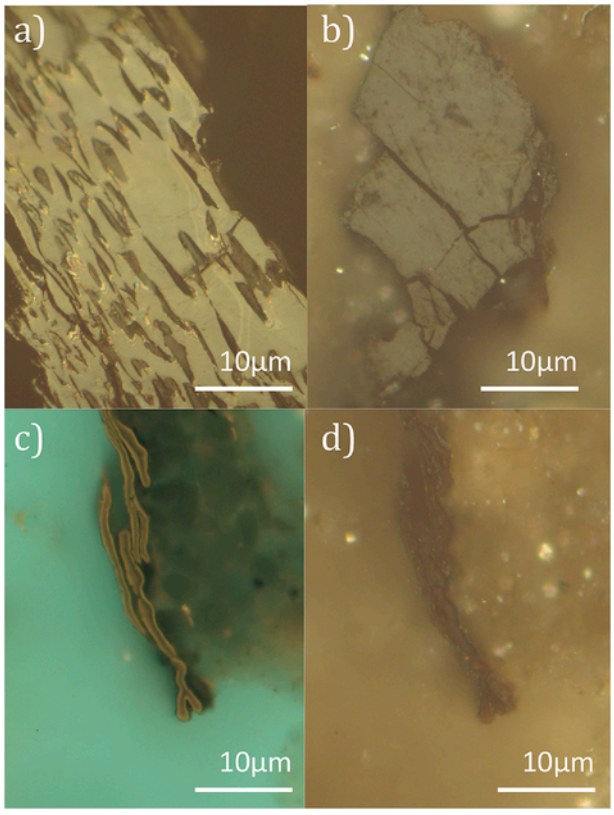

Fig. 2. Microphotographs of macerals detected by reflected light under oil immersion analyses. A) Inertinite fragment; b) vitrinite fragment: c) megaspore under fluorescence light; d) megaspore.

from pale yellow to black. Approximately 50 sporomorphs per sample were examined.

PDI was determined from measurement of the red, green and blue (RGB) intensities of light transmitted through palynomorphs to produce a single greyscale value. In the present study, palynomorphs were digitally imaged using a Leica DM1000 microscope, with a LeicaICC50® with 3.1 mpx resolution digital camera, and LAS EZ® image acquisition software (Goodhue and Clayton, 2010; Spina et al., 2018). Only five samples (HCM17.2, HCM17.3, HCM17.4, HCM17.5 and HCM18.1) weresuitable for PDI analyses according to their palynomorph contents. Approximately thirty spores per sample, each of which covering an area of approximately 16 µm^2, were selected for PDI analysis. The same sporomorphs Calamospora sp., Deltoidospora sp. and Retusotriletes sp., chosen for TAI and SCI, were picked for PDI studies. Images were collected at a constant illumination setting using 40 × magnification. These images were analysed using ImageJ software and the following procedure. The RGB background (Rb, Gb and Bb values) were measured respectively. No photos with values of R, G and B smaller than 247 were utilized to calculate the PDI. Then, the palynomorph interior was selected manually using the Lasso Selection Tool of ImageJ and the RGB values were determined. PDI value was then calculated following the procedure of Goodhue and Clayton (2010),. Based on the PDI values of sporomorphs, the Ro_{eqPDI}% values were determined following the relationship recently proposed by Clayton et al. (2017): Ro_{eqPDI} % = (PDI -11.587)/65.01.

4.2. Micro-Raman

Over past decades, Raman spectroscopy has shown to be a suitable tool for the analysis of carbonaceous material dispersed in rocks. Starting from the pioneering work of Tuinstra and Koenig (1970) that demonstrates the correlation between Raman spectra and the crystal size of graphite, the Raman studies have been refined and optimized with the development of the Raman spectroscopy of carbonaceous material (RCSM) method (Beyssac et al., 2002; Lahfid et al., 2010; Lünsdorf et al., 2017) that calculate maximum paleotemperatures in metamorphic rocks. Nowadays this technique has also been widely recognized as a powerful thermal maturity tools for coals and dispersed kerogen in diagenesis (Kelemen and Fang, 2001; Sadezky et al., 2005; Guedes et al., 2010, 2012; Quirico et al., 2005; Liu et al., 2013; Hinrichs et al., 2014; Wilkins et al., 2014, 2017; Lünsdorf and

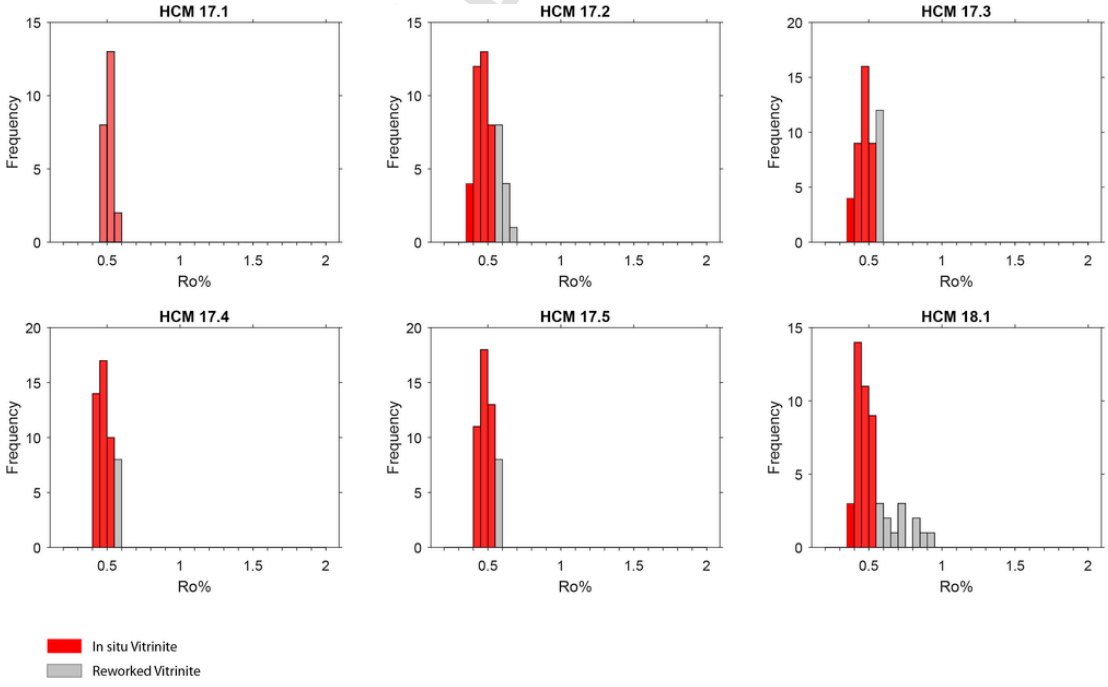

Fig. 3. Reflectance values for the whole set of samples. In red vitrinite defined as *in-situ*, in grey reworked and low reflectance vitrinite. (For interpretation of the references to color in this figure legend, the reader is referred to the Web version of this article.)

Table 2
Average Raman parameters calculated on the sporomorphs and phytopclasts groups for different samples. Acronysms: pD = position of the D band; pG = position of the band; wD = width at half height of the D band; wG = width at half height of the G band; aD = integrated area of the D band; aG = integrated area of the G band; ΔD-G = distance between D and G band; ID/IG = intensity ratio of the D and G bands; aD/aG = area ratio of the D and G bands; wD/wG = width ratio of the D and G bands; Ro% equivalent = vitrinite reflectance equivalent calculated according to Schito and Corrado's (2018) equation; s.d. = standard deviation.

Sample	pD	s.d pD	pG	s.d. pG	wD	s.d. wD	wG	s.d. wG	aD	s.d. aD	aG
HCM 17.2 sporomorph	1372.59	8.40	1610.84	2.28	242.87	34.60	142.53	24.62	15081.53	10427.87	28792.83
HCM 17.2 phytoclast	1362.76	8.49	1611.01	2.49	292.58	43.57	144.90	17.79	30106.76	20359.90	32249.72
HCM 17.3 sporomorph	1383.11	–	1617.48	–	242.92	–	221.23	–	91953.31	–	98974.87
HCM 17.3 phytoclast	1364.72	8.88	1608.95	2.49	292.30	4.05	168.98	6.28	45609.00	17400.36	44863.23
HCM 17.4 sporomorph	1369.95	Err:504	1613.67	Err:504	174.06	Err:504	144.31	Err:504	9075.39	Err:504	18159.22
HCM 17.4 phytoclast	1370.29	10.40	1611.15	1.73	292.82	34.16	148.15	12.39	53338.13	19400.45	51224.89
HCM 17.5 sporomorph	1374.30	7.88	1619.82	5.87	209.69	56.47	125.11	9.65	23069.18	15366.07	28660.01
HCM 17.5 phytoclast	1373.00	3.49	1620.05	2.00	268.22	40.62	141.59	14.65	33102.15	13871.26	35274.25
HCM 18.1 sporomorph	1382.02	3.31	1608.58	4.59	340.87	84.81	163.67	9.96	7468.16	3144.88	7135.12
HCM 18.1 phytoclast	1372.88	6.35	1607.82	2.74	309.65	44.88	142.07	18.11	20077.34	7947.00	17042.50
Sample	**s.d. aG**	**ΔD-G**	**s.d. ΔD-G**	**ID/IG**	**s.d. ID/IG**	**aD/aG**	**s.d. aD/aG**	**wD/wG**	**s.d. wD/wG**	**Ro% equivalent**	**s.d. Ro% equivalent**
HCM 17.2 sporomorph	21638.61	238.25	7.44	0.45	0.08	0.56	0.14	1.72	0.16	0.25	0.10
HCM 17.2 phytoclast	17657.22	248.25	8.67	0.68	0.30	1.11	0.86	2.04	0.37	0.57	0.15
HCM 17.3 sporomorph	–	234.37	–	0.75	–	0.93	–	1.10	–	0.06	–
HCM 17.3 phytoclast	11383.51	244.22	6.39	0.49	0.09	1.00	0.13	1.73	0.09	0.37	0.08
HCM 17.4 sporomorph	13516.19	243.72	8.35	0.41	0.10	0.49	0.13	1.23	0.37	0.23	0.10
HCM 17.4 phytoclast	14735.39	240.86	9.90	0.73	0.24	1.08	0.40	1.99	0.33	0.48	0.12
HCM 17.5 sporomorph	13062.98	245.52	3.50	0.50	0.09	0.76	0.30	1.68	0.48	0.32	0.18
HCM 17.5 phytoclast	10119.50	247.05	1.48	0.54	0.00	0.92	0.13	1.92	0.49	0.51	0.09
HCM 18.1 sporomorph	2474.08	226.56	7.90	0.70	0.02	1.03	0.08	2.07	0.39	0.35	0.07
HCM 18.1 phytoclast	7180.26	234.94	7.17	0.61	0.07	1.19	0.22	2.19	0.31	0.42	0.09

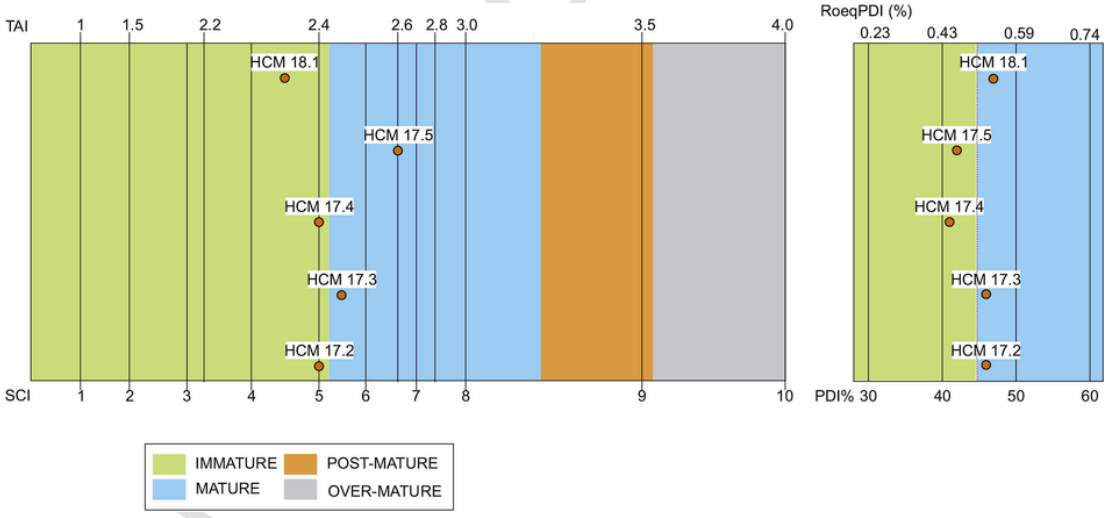

Fig. 4. a) TAI and SCI values plotted against the window of hydrocarbon generation. B) PDI values.

Lünsdorf, 2016; Mum and Inan, 2016; Lupoi et al., 2017; Schito et al., 2017a; Schmidt et al., 2017; Hackley and Lunsdorf, 2018; Schito and Corrado, 2018).

Raman spectra of carbonaceous matter appears in the first order region between 1100 and 1700 cm^{-1} and only for high matured organic matter, in the second order region between 2000 and 3500 cm^{-1}. The first order Raman spectra consists of two main bands known as the D and the G bands (Tuinstra and Koenig, 1970; Friedel and Carlson, 1972) and other minor bands depending on the degree of the coal rank (Li, 2007; Potgieter-Vermaak et al., 2011). The G band is the only Raman active vibration in crystalline graphite at 1582 cm^{-1} (Tuinstra and Koenig, 1970; Reich and Thomsen, 2004; Pimenta et al., 2007) and is related to the in-plane vibration of the carbon atoms in the graphene sheets.

The D band at 1350 cm^{-1} becomes active in disordered graphite and its frequency depends on the excitation laser (Pócsik et al., 1998). Its origin has been interpreted as a results of a double resonant Raman scattering process (Pócsik et al., 1998; Reich and Thomsen, 2004; Pimenta et al., 2007). Alternatively, the collective intensity of the D band has been related to the ring breathing vibration in the graphite

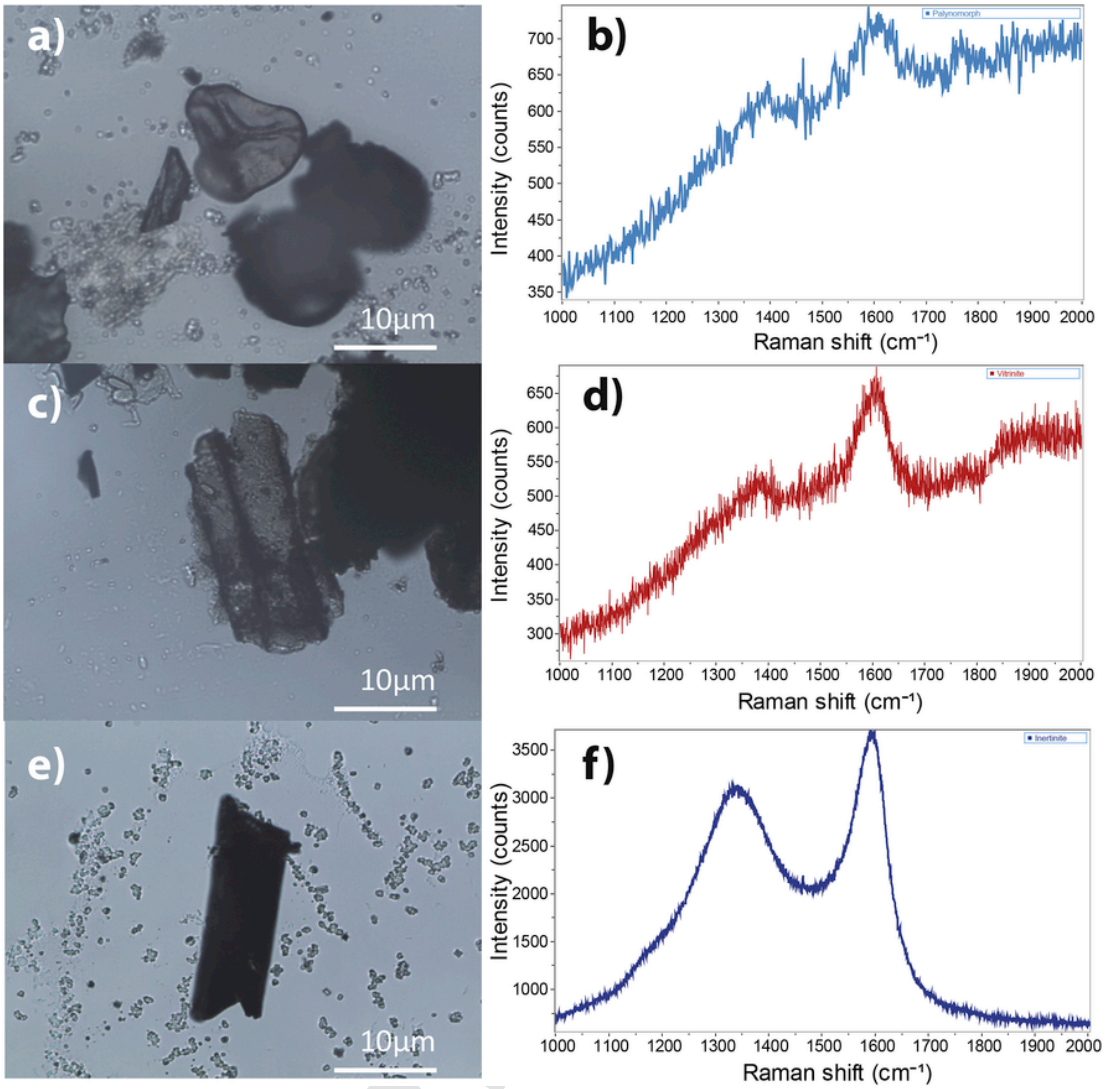

Fig. 5. Microphotographs and associated Raman spectra of: sporomorphs (a–b), translucent phytoclasts (c–d) andopaque phytoclasts (e–f).

sub-unit or polycyclic aromatic compounds (PAHs; Negri et al., 2002, 2004; Castiglioni et al., 2004; Di Donato et al., 2004; Lünsdorf and Lünsdorf, 2016) or to aromatics with 6 rings or more (Li, 2007).

Unlike the G and D band assignment, a general consensus on the chemical meaning of the other spectral features at 1100–1200 cm^{-1} and 1400–1500 cm^{-1} is still missing (Ferralis et al., 2016; Rebelo et al., 2016; Schito et al., 2017a). Moreover, bands at 1465 cm^{-1} and 1380 cm^{-1}, which represent the ''overlap" between D and G, were assigned to mainly amorphous carbon structures in char, especially small ring systems (e.g., with 3–5 fused benzene rings) by Li et al. (2006), Li (2007) and Rebelo et al. (2016).

In this work, micro-Raman spectroscopic analyses were performed on sporomorphs and phytoclasts recognized on strew mounts like those used for palynological analyses. Micro-Raman spectroscopy was carried out using a Jobin Yvon LabRam system in a backscattering geometry. Data were collected in the first order Raman spectrum over the range 1000–2000 cm^{-1} using a 600 grooves/mm spectrometer grating and CCD detector. A Neodimium-Yag green laser (532 nm) was used as a light source. In order to avoid laser-induced degradation of kerogen and reduce the fluorescence background to minimal values, laser power was adjusted below 0.4 mW using optical filters and the Raman backscattering was recorded after an integration time of 20s for 6 repetitions. Each phytoclast or sporomorph was analysed with a 2 µm diameter spot using a 20× or a 50× optical power objective.

Since user interpretation and extrapolation affects the comparability of parameters in the peak deconvolution of Raman spectra of kerogen, as demonstrated by Quirico et al. (2005) and Lupoi et al. (2017, 2018), the present study we applied an automatic fit as proposed by Schito and Corrado (2018), which is particularly suitable for low maturity samples. This method analyses separately the D and G bands regions by performing a linear baseline in the region between 1190 and 1490 cm^{-1} (D band region) and between 1430 and 1690 cm^{-1} (G band region) and then deconvolving each spectra region using two asymmetric Gaussian bands in order to determine intensity and position. The asymmetry of the bands was set at 65% and 60% for the D and G regions respectively. Finally, the area integration of each band region was measured. Raman parameters were finally converted into vitrinite reflectance equivalent using the second multiparametric equation proposed by Schito and Corrado (2018).

Statistical Principal Component Analysis (PCA) and Partial Least Square discriminant analysis (PLS-DA) were performed on traslucent phytoclasts and sporomorphs Raman spectra, in the full wavenumber range (1000-2000 cm^{-1}). The main purpose of PCA analyses is to explain the variance-covariance structure of the data using a linear combination of the original variables to form principal components (PC).

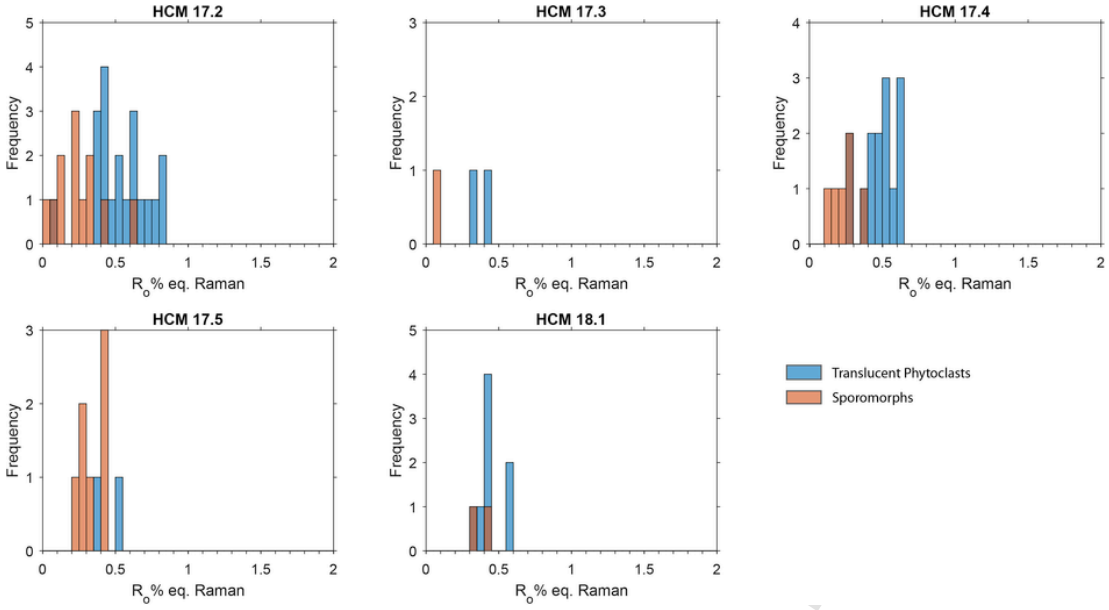

Fig. 6. Histograms of Ro equivalent values from Raman parameters. In blue Ro equivalent values for translucent phytoclasts, in red for sporomorphs. (For interpretation of the references to color in this figure legend, the reader is referred to the Web version of this article.)

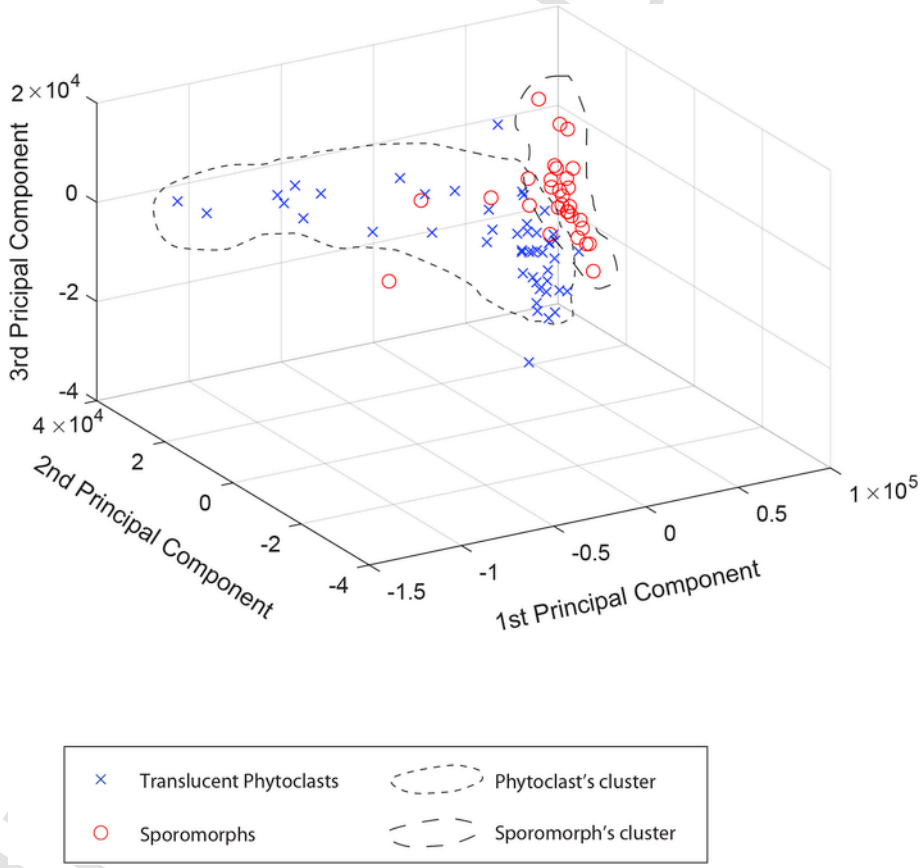

Fig. 7. 3D plot of PC1, PC2 and PC3. Blue cross represents translucent phytoclasts, while red circle denote sporomorphs. (For interpretation of the references to color in this figure legend, the reader is referred to the Web version of this article.)

By finding combinations of the original dimensions that describe the largest variance between the datasets, complete information from the original dataset can be taken into account by a smaller number of variables. In this work we adopted PCA analysis to project the original data into a space that maximizes the variability and thus examines the qualitative differences within translucent phytoclasts and sporomorphs data in the PC space, taking into account also that internal hetereogeneities of each organic fragment could exist (Jubb et al., 2018).

Partial Least Square discriminant analysis (PLS-DA) was used to develop classification rules for unknown macerals. In detail, we separated

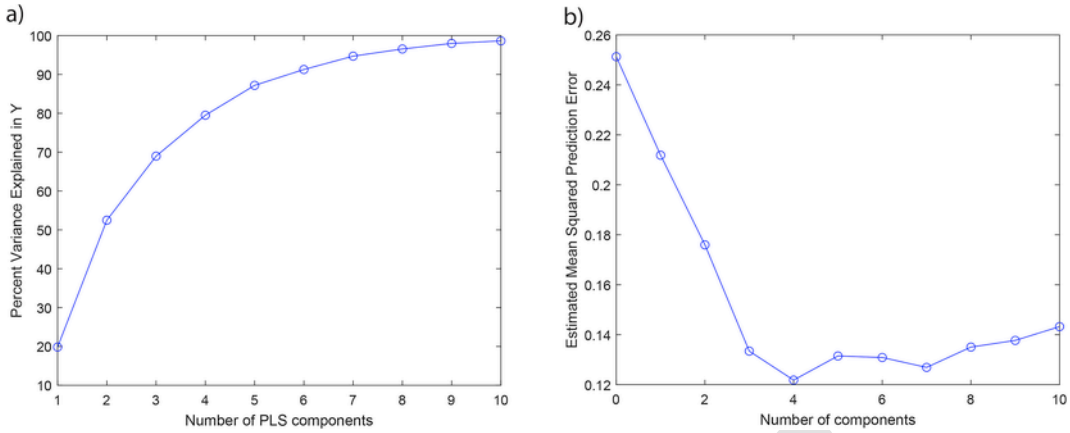

Fig. 8. a) Percent of variance expressed by the normalized intensity of each Raman spectra (y) and b) number of PLS components.

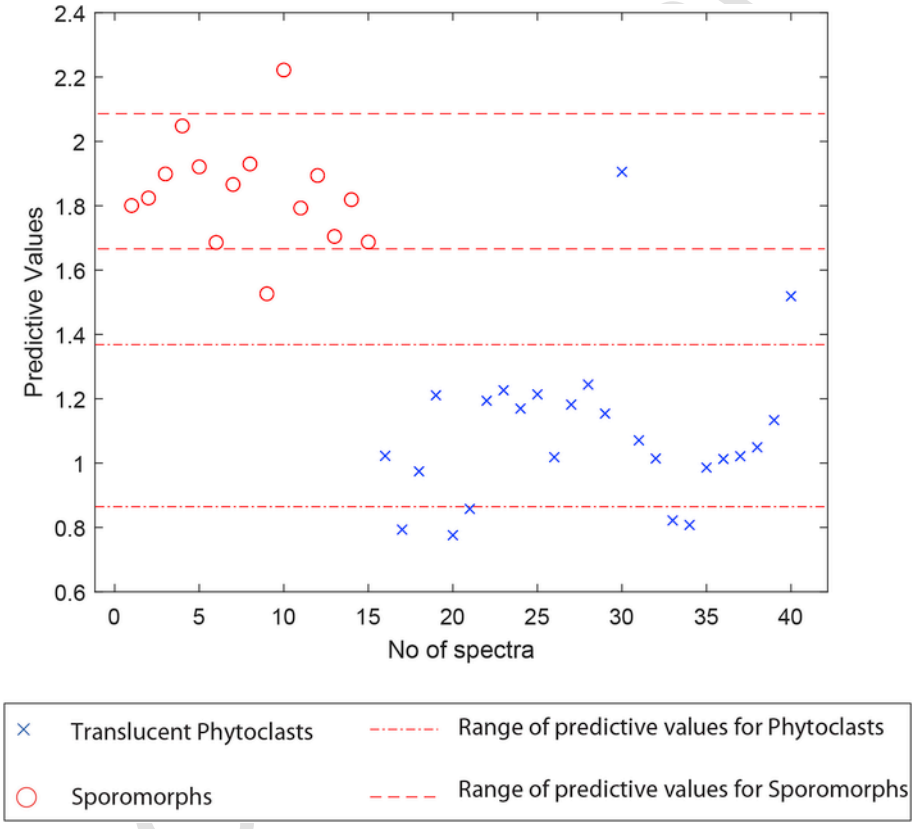

Fig. 9. The diagram shows the relationship between predicted PLS values calculated for phytoclasts (blue crosses) and sporomorphs (red circles) for the testing set and the predicted values of phytoclasts (dash-dot line) and sporomorphs (dashed lines) calculated in the training set. The x axis represents the number of spectra that belong to the sporomorphs group (from No. 1 to 15) and to the translucent phytoclasts (from No. 16 to 39). (For interpretation of the references to color in this figure legend, the reader is referred to the Web version of this article.)

the whole dataset into two groups, the training and testing sets. The training set was used to develop a calibration model and find the predicting parameters that were used to classify the testing set. PLS-DA performed for the training set, unlike PCA, does not use only the raw spectra (independent variables), but also an external a priori classification (dependent variable). This method considers the whole data as two different groups (named group 1 for the translucent phytoclasts and group 2, for thesporomorphs) based on the external knowledge. The model calibration produces a set of regression coefficients from which the predicted values of the dependent variables are computed. The relation between independent and dependent variables in the training set is given by the beta coefficients. Working on the testing set, the beta coefficient multiplied by the independent variables allows to predict the unknown dependent variables.

Before performing PCA and PLS-DA all spectra were preprocessed for spike removal and spectra normalization. The PCA routine of MATLAB software (The MathWorks, Natick, MA) was used.

5. Results

5.1. Palynofacies and Sporomorph assemblage

The organic fraction consists only of terrestrial organic debris, due to the continental nature of the depositional environment (Pienkowski,

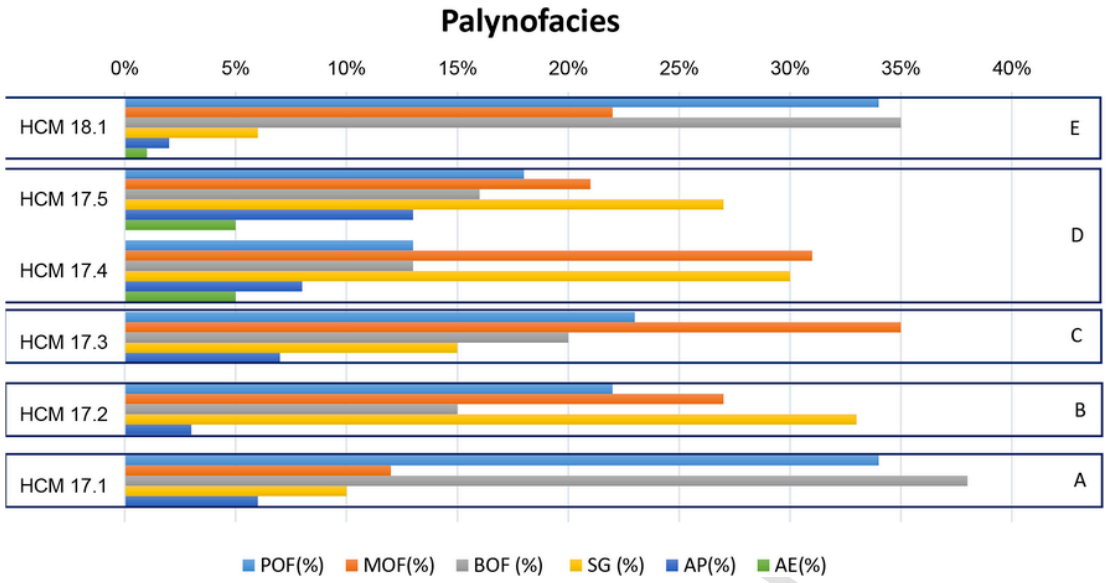

Fig. 10. Relative abundance of selected organic parameters of palynofacies from analysed samples. Acronyms: POF = dark brown, partially oxidized fragments translucent fragments; MOF = Cell-structured orange to dark brown, moderately oxidized, fragments; BOF = Black opaque completely oxidized fragments; SG = Sporomorphs including spores and pollen; AP = amorphized phytoclasts; AE = aquatic elements. (For interpretation of the references to color in this figure legend, the reader is referred to the Web version of this article.)

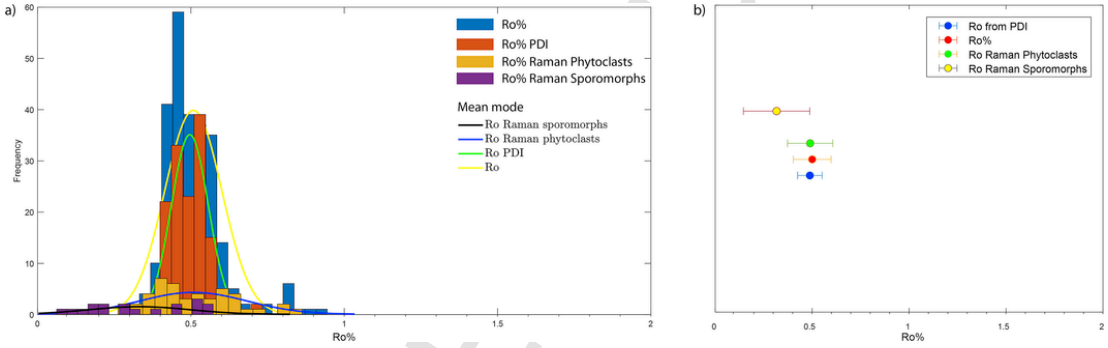

Fig. 11. a) The histogram compares Ro measure on vitrinite (blue bins), with the Ro equivalent calculated from PDI according to Clayton et al. (2017) equation (red bins) and Ro equivalent from Raman parameters calculated on translucent phytoclasts (yellow bins) and sporomorphs (purple bins). Coloured lines represent the normal mode distribution of the different parameters. B) Average values and standard deviations form Ro values measured on vitrinite in red, Ro equivalent from PDI in blue and Ro equivalent from Raman parameters calculated on translucent phytoclasts in green and sporomorphs in yellow. (For interpretation of the references to color in this figure legend, the reader is referred to the Web version of this article.)

2004). The overall palynofacies mostly contains structured organic matter (SOM) with different degree of preservation and unstructured organic matter (UOM, Fig. 2).

For details on the terminology adopted for palynomacerals see the supplementary online material.

The SOM group includes:

- Completely oxidized black opaque fragments (BOF; PM4 equivalent). This type of palynomaceral is very resistant and can be transported over a long distance before being degraded (Tyson, 1995).
- Translucent orange to dark brown partially oxidized fragments (POF; PM1 equivalent), without visible original cellular structures. This group also includes non-structured charcoal fragments.
- Cell-structured orange to dark brown moderately oxidized fragments (MOF; PM2 + PM3 equivalent) including pale, cell structured yellow to dark orange fragments of mainly cuticular origin (e.g., preserved leaf and stem cuticle) and structured charcoals, commonly showing tracheidal structures.
- Sporomorphs. This group includes spores and pollen of land plants (SG).
- The only recorded aquatic elements (AE) are *Botryococcus* sp. a fresh and brackish Chlorococcale alga of coastal lakes and lagoons (Batten and Grenfell, 1996). It can be also found in temperate or tropical oligotrophic lakes and estuaries, and it blooms in presence of high levels of dissolved phosphorus (Warren, 1986; Tyson, 1995).

Most UOM consists of amorphized phytoclasts (AP) appearing as reddish flakes with diffuse but recognizable outlines and, sometimes, residual internal structures. Occasionally, in a few levels, palynofacies contain also gelified debris showing more homogeneous texture, from brownish to orange coloured, and marked outlines. AP and gelified debris derive by the *in situ* decay of plant fragments (Van der Zwan, 1990), at various degradation stages. In particular, the gelified debris has been considered as a result of submerged and semi-emerged macrophyte degradation within the water column (Sifeddine et al., 1995; Martín-Closas et al., 2005). Moreover, UOM represented by highly amorphous and fluorescent material, probably derived from algae degradation, is extremely rare.

The sporomorph specimens are abundant, well preserved and rather diversified. *Classopollis torosus* and *Classopollis* sp. are common in all samples with the exception of HCM 17.1. Spores *Calamospora mesozoica*, *Calamospora* sp., *Deltoidospora toralis*, *Deltoidospora* sp., *Dictyophyllidites harrisi*, *D. mortonii*, *Duplexisporites problematicus*, *Retusotriletes* sp., *Trachysporites fuscus* are commonly present in all samples.

Cerebropollenites macroverrucosus, *C. thiergartii*, *Conbaculatisporites mesozoicus*, *Contignisporites problematicus* and *Uvaesporites argentiformis* are abundant in most samples with the exception of HCM 17.3 where only smooth spores were found. Bisaccate pollen grains (i.e *Alisporites* spp., *Vitreisporites pallidus*) are less common.

The palynological composition confirms a Hettangian age for the investigated portion of the Zagaje Formation (Pieńkoski, 2004; Pienkowski and Waksmundzka, 2009; Pieńkowski et al., 2012), highlighted by the presence of *C. thiergartii*, considered as the best palynological marker for the base of the Jurassic System. In the GSSP Kuhjoch section (Karwendel Mountains, Austria), the FAD of the species index *C. thiergartii* has been recorded several meters below the first appearance of the ammonite *Psiloceras spelae*, marking the base of the Hettangian (Bonis et al., 2009; Kürschner and Herngreen, 2010; Hillebrandt et al., 2013).

The presence of Cheirolepidiaceae pollens (e.g., *Classopollis* sp.) and fern-producing spores (e.g., *Deltoidospora mesozoica*, *Dictyophyllidites mortonii*, *D. harrisi*, *Trachysporites fuscus*) indicates a general warm-humid climate, as already postulated in previous papers (i.e., Pieńkowski et al., 2012 for references). Evidences of a global increase in humidity starting from Late Triassic are largely documented by several authors and have been related to the degassing of basaltic flows from the Central Atlantic Magmatic Province (Cirilli et al., 2009, 2018; Van de Schootbrugge et al., 2009; Bonis et al., 2010; Schoene et al., 2010; Ruhl and Kürschner, 2011; Schaller et al., 2011; Lindströ;m et al., 2017; Davies et al., 2017).

5.2. Thermal maturity

Observed under reflected light, all samples show a very rich and heterogeneous organofacies composition (Figs. 2 and 3). Most fragments observed under oil immersion show fusinite-like textures with high relief and reflectance values, comprised between 0.90 and 1.60 R_o% (Fig. 2a). These fragments are not present in the histograms in Fig. 3. Most of these fragments are probably charcoal derived from Jurassic wildfire, as already outlined by Marynowski and Simoneit (2009).

The huminite-vitrinite group generally shows lower reflectance values between 0.45 and 0.60% (Figs. 2b and 3) with a normal distribution centered at the 0.50 R_o% class. This group is sometimes made up of different vitrinite groups and/or sub-macerals groups. As shown in Table 1, *in situ* vitrinite reflectance (R_o%) shows values between 0.51 and 0.47 with standard deviations between 0.02 and 0.04. Nevertheless, other vitrinite fragments with higher reflectance between 0.55 and 0.80 are also present and probably represent a reworked population. This is particularly evident in samples 18.1 and 17.2 (Fig. 3). Moreover, some small fragments showing dispersed and low reflectance, were detected in samples 17.2, 17.3 and 18.1 (Fig. 3) with R_o% of about 0.35. These low-reflectance fragments could be tentatively interpreted as vitrodetrinite or desmocollinite, but given the difficulties of their identification in dispersed organic matter we'll consider them as vitrinite.

In Table 2, the mean reflectance values of all submacerals of the huminite-vitrinite group is set as Ro_{tot} % while the column R_o% refers only to the *in situ* vitrinite. In detail, samples HCM17 show mean reflectance values at about 0.5%. Macerals of the liptinitic group were also recognized showing a yellowish-brownish fluorescence when excited in blue fluorescent light (Fig. 2c and d).

Both TAI and SCI methods suggest that only two samples (i.e. HCM17.3 and HCM17.5) fall within the oil window (mature stage of HC generation). On the other hand, the remaining samples (i.e. HCM17.1, HCM17.2 and HCM18.1) fall within the biogenic gas window, very close to the onset of the oil window.

Placing the samples in stratigraphic order, no vertical trend in PDI values is observed from the analysed sporomorphs (Table 1, Fig. 4). PDI values vary from 41 (lowest value for sample 17.4) to 47% (highest value for sample 18.1). The mean vitrinite reflectance equivalent from PDI (Ro_{eqPDI}%) ranges from 0.45 to 0.54% with an average of 0.50%. No data were obtained for sample HCM17.1 due to the scarcity of sporomorphs.

5.3. Micro-Raman on phytoclasts and sporomorphs

Unornamented and unfolded sporomorphs are easily identified by their morphology (Fig. 5a). As far as phytocalsts are concerned, two distinct classes of phytoclasts are recognized. Both classes generally show an elongated shape: the first class is totally opaque (Fig. 5 e), while the second is translucent (Fig. 5 c). Opaque fragments belong to BOF and correspond to the inertinite group recognized in the reflected light analyses. They were not considered for thermal maturity conversion. UOM in form of highly amorphous and fluorescent material was also recognized under transmitted light, but its Raman signal is highly variable due to the heterogeneity of its internal composition (Taylor et al., 1998) and was not considered in the thermal maturity assessment. From a qualitative point of view, a difference exists between Raman spectra of palynomorphs and translucent phytoclasts (Fig. 5 b,d,f). Raman spectra of sporomorphs generally show higher fluorescence background and a wider G band as compared to vitrinite spectra (Fig. 5b and d). For the sake of comparison, a spectrum of opaque phytoclasts is shown in Fig. 5 f. It displays very low fluorescence, a narrower G band and the D band shifted to lower wavenumbers.

Mean values of Raman parameters measured on translucent phytoclasts and sporomorphs for each sample are listed in Table 2, while values for single fragments are listed in Table A (see supplementary materials). In general, it can be observed that while the G band position in both sporomorphs and phytoclasts is almost identical within error, with an average value at about 1610 cm^{-1}, the position of the D band is generally slightly shifted toward higher wavenumbers for sporomorphs. This, for most of the samples, results in higher Δ D-G values for phytoclasts compared to sporomorphs (Table 2). The width of the G band (wG) is the same for both maceral classes, while the D band width (wD) as well as the width and area ratio are systematically higher for phytoclast fragments. Analogously, the intensity ratio shows higher values for phytoclasts than other fragments.

The average Ro equivalent values ($Ro_{eqRaman}$%) span between 0.25 and 0.35 for sporomorphs and between 0.35 and 0.57 Ro% for phytoclasts with a main mode centered at about 0.50 R_o% for the last group (Fig. 6).

5.4. PCA and PLS-DA on Raman spectra

In this work PCA analysis was used for a preliminary data overview in order to define groups, relationships among groups and possible outliers. The first three principal component account for about the 94% of the variation among Raman spectra. In detail the first principal component (PC1) represents the 79% while PC2 and PC3 account for the 13% and 2% respectively.

In Fig. 7, a 3D plot of PC1, PC2 and PC3 for the sporomorph and translucent phytoclasts groups defined respectively by red circles and blue crosses is presented. Based on the combination of the three PCs it is possible to differentiate the two groups as outlined by the dashed and dashed-point lines. The two groups show the highest density of points in close proximity, but still very distinct. In addition, it is possible to observe a larger spread of phytoclasts spectra and the presence of perhaps three sporomorph spectra falling in the PC range of phytoclasts. PLS-DA was used in this work to develop predicted parameters for classification of the testing set of Raman spectra. The training and testing set of samples were prepared building two matrixes composed by half of the spectra chosen randomly starting from the original

dataset. To build the calibration model we used four factors that account for about 80% of the variance expressed by the dependent variable (Fig. 8a). The mean squared predicting error for the calibration (MSPE) is 0.12 and represents the error that can be expected when predicting unknown variables (Fig. 8b). Fig. 8a and b indicate that a statistically significant number of PLS components for the training model is four, since it explains a high percent of variance with the minimum error. Introducing more components in the model could lead to overfitting. Overfitting occurs whenever the model matches too closely the data and the information cannot longer be differentiated from the random noise. In Fig. 9, the results for the testing set for the two groups (red circles and blue crosses) are presented where the number of spectra that belong to the sporomorph group (from 1 to 15) and to the translucent phytoclasts (from 16 to 39) are presented versus the ranges of predicted values for the two groups found in the training set. Samples from the testing set are in good agreement with the ranges previously calculated since only six phytoclasts and one sporomorph spectra fall out of the respective ranges.

6. Discussion

6.1. Palynofacies and organic facies

Although there are only a small number of samples (5 samples) a palynofacies analysis along with geochemical data has been carried out as a methodological approach to characterize the depositional environment. Palynological analysis led to the recognition of five palynofacies types (A, B, C, D, E; Fig. 10) defined on the base of:

- the percentage of the most common organic debris;
- the preservation/degradation degree of sporomorphs and palynodebris which is essentially a function of oxidation and sedimentation rate;
- the presence/absence of UOM as an index of redox conditions in the water column and sediment–water interface.

Palynofacies A (Fig. 10 and Figs. 1 and 2 in Plate A), recorded in sample HCM17.1, is dominated by POF and BOF, including black, unstructured charcoal fragments. Also present are moderate amounts of sporomorphs and accessory amorphized phytoclasts (AP). The sample shows low HI and TOC values, which prevents the accurate determination of Tmax from Rock-Eval Pyrolysis.

Palynofacies B (Fig. 10 and Figs. 3 and 4 in Plate A), from HCM 17.2 sample, shows a higher content of sporomorphs associated to a moderate amount of POF and MOF and low BOF, including black, unstructured charcoal fragments. The high TOC value suggests a higher OM sedimentation rate. Under this condition, the OM is quickly buried and removed by the sediment/air or sediment/water interface where the oxidation processes are stronger.

Palynofacies C (Figs. 10 and 5 in Plate A), in the sample HCM 17.3, contains abundant MOF, including charcoal tracheids, moderate percentage of POF, BOF, and minor sporomorphs. The peculiarity of this palynofacies consists of a relative abundance of amorphized phytoclasts, part of them gelified. The low TOC and HI values suggest a lower OM sedimentation rate and poor conditions of preservation.

Palynofacies D (Figs. 10 and 7 in Plate A), yielded from the samples HCM17.4 and HCM17.5, is dominated by sporomorphs and MOF with minor BOF and POF. Sporomorphs are frequently riddled by pyrite, which has been found also as framboidal crystals in the organic residue. Amorphized phytoclasts, some of which attached by fungal hyphae and the alga *Botryococcus* sp. (Fig. 9 in Plate A), are relatively abundant with respect to other palynofacies. Structured charcoal, showing tracheidal structures (Fig. 10 in Plate A), is also present. The palynofacies type and the presence of *Botryococcus* are in agreement with the highest HI value.

Palynofacies E (Fig. 10 and Figs. 11–13 in Plate A), recorded in the sample HCM18.1 is dominated by degraded palynomacerals as BOF, unstructured charcoal included, and POF, moderate MOF and low amount of sporomorphs. The TOC value, which is the highest recorded, should suggest a high OM sedimentation rate within a strongly oxidizing environment as revealed by the palynofacies type and by low HI value.

Overall, the nature of palynofacies confirms a terrestrial aquatic environment (as suggested by Pienkowski, 2004) for the exclusive presence of continental organic debris, fresh water algae and absence of marine organisms. The organic matter abundance and preservation implies short transport distances and indicates a lacustrine to swampy (palustrine) depositional environment. The absence of exclusively brackish organisms excludes, at least for the studied sedimentary interval, a coastal lake. The deposited organic matter thus originates from higher plants that grow in the immediate vicinity of the lake, as testified also by the great sporomorph diversity and by the presence of preserved leaf and stem cuticle. The cuticular fragments are less resistant to physical and biological degradation and thus are rarely preserved in high-energy depositional environments that involve reworking of sediments and indicate therefore short distance of transportation.

By comparison in the palynofacies with TOC and HI values, the variation of organic facies can be related to alternate periods of reducing/oxidizing conditions and of different sedimentation rates in the depositional environment. Reducing conditions are evident in the palynofacies D, marked by the presence of pyrite and amorphized phytoclasts, gelified debris included. In this palynofacies, the highest values of HI can be related also to the presence of *Botryococcus* sp., abundant sporomorphs and to the low amount of strongly oxidized organic matter. Reducing conditions probably prevailed in stagnant water body where the recharge of fresh water was scarce or absent and also the sedimentation rate not very high, as documented by the lower value of TOC.

Moreover, the OM sedimentation rate seems to fluctuate and periods characterized by high TOC value (i.e palynofacies B and E) are alternating to periods recording very low TOC (palynofacies A, C). However, the low HI values of palynofacies B and E suggest oxidation processes strong enough to degrade the OM. The fluctuation of OM sedimentation rate is probably related to the periodic fluctuation of the lake levels that exposed bottom sediments to oxygenated surface water during low water-level periods. This created oxidizing conditions that reduced the abundance and preservation of the organic particles in the sediments.

Finally, charcoal remains (POF and BOF, particularly abundant in palynofacies A, B and E) have been recorded also by previous authors (Pienkowski and Waksmundzka, 2009; Marynowski and Simoneit, 2009; Belcher et al., 2010; Pieńkowski et al., 2012) and related to forest fires occurring on the surrounding lands.

6.2. Thermal maturity

Working on the POF group under reflected light, indigenous vitrinite shows mean reflectance values between 0.47 and 0.51%. Vitrinite with higher values mainly between 0.60 and 0.90% (Fig. 3 and Table 1) was found and has been interpreted as reworked vitrinite. Lower reflectance values at around 0.35–0.40%, on the other hand, were found for small detrital vitrinite fragments and/or for more homogeneous, unstructured and slightly fluorescent small fragments that could probably be interpreted as desmocollinite or vitrodetrinite. These last macerals probably correspond to the amorphized phytoclasts (AP) observed under transmitted light. The amorphization, according to Tyson (1995) can be due to anaerobic decomposition of land plants. This process led

to the production of intra and extracellular amorphous material that lowers the reflectance.

Thermal maturity assessment by means of optical analyses under transmitted light, performed on the sporomorph group (SP), generally confirmed the maturation level determined by R_o% results on the indigenous vitrinite. As illustrated in Fig. 3, SCI, TAI and PDI almost always lie at the onset of the oil window. The only difference is that while the R_o% values for samples 17.2, 17.3, 17.4, 17.5 and 18.1 are almost fixed at an average value of 0.47, a bigger spread is shown by TAI and SCI, in particular for samples 17.5 and 18.1. At the same time PDI-based R_o% equivalent values spread between 0.45 and 0.54% (Table 2), a wider range with respect to that of indigenous vitrinite reflectance. This is consistent with oil-prone materials like amorphous organic matter or palynomorphs that generally follow a maturation pattern characterized by discrete jumps rather than a regular increase as reflected by the discrete jump in color alteration (CAI, AAI, TAI, SCI).

The calculated thermal maturity is also confirmed by vitrinite reflectance data and Tmax data performed by previous works on the same outcrops (Marynowski and Simoneit, 2009; Schito et al., 2017b).

6.3. Raman analyses

6.3.1. Raman parameters and vitrinite reflectance equivalent

In general, differences between phytoclasts and sporomorph can be chemically described in terms of H/C ratio. At microscopic level this difference can be expressed by a different optical behaviour (low reflectance values and generally high fluorescence for sporomorphs) or by means of micro FT-IR spectroscopy.

Raman spectroscopy is a powerful tool to detect changes in aromatization in OM at different coal ranks (Hinrichs et al., 2014; Wilkins et al., 2014; Mum and Inan, 2016; Zhou et al., 2016; Schito et al., 2017; Schmidt et al., 2017; Lupoi et al., 2018; Schito and Corrado, 2018) or between different components of kerogen (Schmidt et al., 2017; Wilkins et al., 2018).

Despite the extensive literature, no attempts have been made to study differences of Raman spectra between translucent phytoclasts and sporomorphs even if it has been already demonstrated that the Raman spectra of hydrogen rich kerogen can be successfully used in thermal maturity assessment (Schito et al., 2017a; Schito and Corrado, 2018). To reach this goal we decided to analyze samples at the same maturation level in order to have a significant number of spectra from both phytoclasts and sporomorphs to compare. Particularly, one of the main tasks was to find sporomorph specimens that are intact, smooth and display no ornamentations to obtain reliable Raman spectra. In addition, a very strong fluorescence (probably enhanced by low maturity and by the glass slide used for transmitted light observations) and the texture inhomogeneities of the material (Jubb et al., 2018), made even more difficult the spectroscopic analysis of sporomorphs.

Despite the aforementioned difficulties we managed to obtain 10-30 spectra for each sample except for the sample HCM17.1 because it was impossible to concentrate material for the strew mount due to its low TOC.

Concerning the translucent phytoclasts, Raman analyses under transmitted light were mainly focused on the POF and tentatively on the AP fraction of the whole kerogen. According to reflected light observations the POF fraction could be related to both to the *in situ* and reworked vitrinite, while the AP fraction probably related to the low reflectance vitrinite. Palynofacies B and D were found most suitable for this work due to their high content of sporomorphs, while palynofacies C and E, due to the abundance of amorphized phytoclasts and a generally low percentage of sporomorphs were more difficult to analyze and gave more uncertain results.

The first feature that characterizes sporomorphs is the very high fluorescence in Raman spectra. Such a high fluorescence generally has a strong influence on spectra interpretation. However, as the equation proposed by Schito and Corrado (2018) on concentrated kerogen is already calibrated for spectra with high signal to noise ratio, we were able to analyze these high fluorescence spectra.

Concerning Raman parameters, as shown in Table 1 and Plate A (supplementary materials), the main differences among phytoclasts and sporomorphs reside in the position, width and area of the D band. As far as D position is concerned, a shift toward lower wavenumbers is observed for phytoclasts. According to Ferrari and Robertson (2000) this shift can be attributed to the increase of larger aromatic clusters passing from disordered to more ordered materials. On the other hand, no such differences were found for the G band position, in agreement with observations by Schito et al. (2017a) and Schito and Corrado (2018) who noted that an appreciable shift in the G band position is visible only when samples with very different aromatization degrees are compared (e.g. very immature compared to very mature samples in the diagenetic realm). As a consequence, the D-G distance tends to be generally higher for phytoclasts (Table A, supplementary materials). The D band area and width appear to be the most sensible parameters showing higher values in phytoclasts compared to sporomorphs. This is in agreement with results from Schito et al. (2017a) who also observed an increase of the D band area and width at increased maturation levels. On the other hand, no clear differences were found in the G band area and width within the two groups.

The aforementioned spectral features produce systematically higher values for phytoclasts compared to sporomorphs, in the intensity, area and width ratio of the D and G bands (Table 2 and Table A in supplementary materials), which have shown to be good indicators of the aromatic degree in diagenesis (Guedes et al., 2010; Schito et al., 2017a; Schmidt et al., 2017). The differences in Raman parameters indicate a higher degree of aromatization for the lignin-cellulosic tissues of the phytoclast group with respect to the sporopollenin composition of sporomorphs, confirming results from micro-FTIR analyses by previous authors (Yule et al., 2000; Marshall et al., 2005; Chen et al., 2012).

All the differences in Raman parameters discussed above, parallel the differences in the vitrinite reflectance equivalent (Fig. 6) calculated by means of Schito and Corrado's equation 2 that shows lower values for the sporomorph group.

It is important to stress here that the equivalent reflectance values calculated for the sporomorphs have no maturity meaning and they are used only to stress the differences in aromaticity with respect to phytoclasts. It will be interesting in further studies to calculate a new correlation between sporomorphRaman parameters and thermal maturity using alternative methods like the PDI.

Regarding vitrinite reflectance equivalent calculated on phytoclasts we can observe that for samples where it was possible to obtain a large number of measurements (samples HCM 17.2, 17.4 and 18.1), the average values lie always at around 0.50% (Table 2), confirming the multi-method maturity assessment. Higher $Ro_{eqRaman}$ values are probably attributed to the reworked fraction of vitrinite as evidenced by optical observation.

On the other hand, it is also observed that the lowest reflectance equivalent values in Fig. 6 for both sporomorphs and phytoclasts were mostly found in amorphized fragments. Similarly, Schmidt et al. (2017) also observed at low maturity a systematic downshift of Raman derived thermal maturity parameters like the D-G distance or the area and width ratio of the D and G bands where measurements were taken in degraded phytoclasts that they called “pseudo-amorphous phytoclasts”. This observed low aromaticity in amorphized fragments is probably due to the presence of sub-microscopic fine lipoid intercalations derived from the anaerobic microbiological decomposition of cellulose or sporopollenin.

6.3.2. PCA and PLS-DA on Raman spectra

PCA-PLS methods have been recently proposed as unbiased approaches to detect thermal maturity from Raman spectra in diagenesis (Bonoldi et al., 2018; Lupoi et al., 2018). These authors demonstrated how it is possible to carry out predictive parameters from PLS regression calibrated against a dependent variable represented by R_o%. This is possible since the main changes in Raman spectra occurring in the spectral range between 1350 and 1600 cm^{-1}, are related to chemical modification of kerogen as thermal maturity increases, like an increase of aromatics with more than six rings and a decrease of small size aromatics and amorphous carbon (Bonoldi et al., 2018; Schito et al., 2017a). Given that similar changes also reflect the differences in Raman spectra among palynofacies, as discussed above, it is possible, in the same maturity range, to calibrate the PLS model against a categorical dependent variable (in this case the sporomorph or phytoclast groups).

Before performing PLS-DA, a PCA analysis allows to have an overview on the variance of the whole dataset. Fig. 7 shows that the groups cluster close to each other near the zero value on the 1st PC axis. The overlapping points represent the amorphized phytoclasts or sporomorphs with the highest $Ro_{eqRaman}$ values in Fig. 6. Furthermore, it can be observed that the translucent phytoclasts group have a larger spread than the sporomorphs.

This is because the first principal component with lowest values represents the reworked vitrinite with the highest R_o% and $Ro_{eqRaman}$ values. The PLS-DA model is able to discriminate between the two groups better than the PCA model. The errors within this model can be explained by the presence of amorphized sporomorphs and phytoclasts and of highly matured vitrinite (Fig. 9).

Here we provide a first example of palynofacies prediction and we stress that such prediction can be performed only in samples at the same thermal maturity and with a very similar maceral and palynomorph/sporomorph content. Although preliminary in its nature, this work represents a very important first step to demonstrate how machine learning techniques can be a powerful support in organic petrographic and palynological analyses.

6.4. Final remarks on thermal maturity indicators

Raman spectroscopy and PDI assessment are relatively new techniques that can provide a valid alternative to measure thermal maturity when pitfalls in vitrinite reflectance occur or in the assessment of oil-prone source rocks where phytoclasts are not abundant.

This work demonstrates that thermal maturity assessed by means of different methods (i.e., vitrinite reflectance, PDI and Raman parameters on phytoclasts) provides the same degree of maturation expressed by different parameters (e.g., R_o%, PDI, $Ro_{eqRaman}$, TAI, SCI; (Fig. 11a and b). This is beatifully expressed by the comparison shown in Fig. 11, where Ro%, RoeqPDI and RoeqRaman for sporomorph and phytoclast values are presented in a synoptic view. The resultant histograms shown in Figs. 11a and 11b indicate that the mean modes of the Ro%, RoeqPDI and RoeqRaman values for phytoclasts are all centered at the same values of about 0.50%.

On the other hand, we can clearly demonstrate from Fig. 11a and b that Raman analyses on sporomorphs generally yelds smaller Ro% equivalent values with a significant dispersion. As stated earlier for PDI measurements, dispersion can be due to the presence of amorphized sporomorphs in the palynofacies assemblage and also possibly attributed to the discrete jumps in maturation path of sporomorphs. Moreover, even if we paid special attention measuring only smooth, unfolded, unornamented sporomorph with no thickened walls, it cannot be excluded that the thermal maturity dispersion for sporomorphs derived from internal texture variability, which is also outlinedby Jubb et al. (2018) in AOM and bitumen fragments and/or from the uncertainties derived from the high fluorescence in Raman spectra.

Thus, more studies are needed on this topic, in particular to verify the dependency of standard deviation on the different reactions of various groups of sporomorphs/.

7. Conclusions

In this work we performed detailed analyses on the palynological assemblage and thermal maturation on six samples collected in a Jurassic terrestrial environment at the border of the Holy Cross Mountains in Central Poland.

Palynological analysis led to the recognition of five palynofacies types, and the relative abundances and variations in percentage of the most common organic debris, the preservation/degradation degree of sporomorphs and palynodebris and the presence/absence of UOM indicate an alternation of periods of reducing/oxidizing conditions and different sedimentation rates in a lacustrine depositional environment.

Different thermal maturity indicators were used to define the maturation of the samples, which show no significant variation and lie just at the onset of the oil window.

Thermal maturity data were then compared with R_o % equivalent values derived from Raman analyses performed on phytoclasts and sporomorphs according to the equation proposed by Schito and Corrado (2018). The results show that $Ro_{eqRaman}$ of phytoclasts is consistent with the calculated thermal maturity, whereas sporomorphs show systematically a low degree of aromatization expressed by lower $Ro_{eqRaman}$ values with a higher dispersion.

It is well demonstrated that a multivariate PCA and PLS-DA analysis performed on Raman spectra allow us to highlight and predict the differences among different palynofacies groups in organic matter.

Acknowledgments

We are greatly indebted to Eni for providing fundings for field trip in Poland in 2016. This research was funded by: MIUR Roma Tre Post-doctoral Grant (2017–2020) n° rep. REP. 22 - PROT. 219 of the 26/01/2017and Fondo Ricerca di Base 2018 (SPIRICBAS2018), Department of Physics and Geology, University of Perugia. Moreover, the Grant of Excellence Departments, MIUR (ARTICOLO 1, COMMI 314–337 LEGGE 232/2016), is gratefully acknowledged.

Organic matter characterization by means of petrography in reflected light and Raman spectroscopy and data treatment have been performed at "Roma Tre" University in the Academic Lab of Basin Analysis and Experimental Volcanology and Petrology. Organic facies characterization and PDI evaluation have been performed in the Sedimentary Organic Matter Laboratory of the University of Perugia. We are deeply grateful to one anonymous reviewer, Paul Hackley, the associated Editor Hui Tian and the Editor-in-Chief Qinhong Hu for detailed revisions and helpful suggestions that contributed to improve the original manuscript.

Appendix A. Supplementary data

Supplementary data to this article can be found online at https://doi.org/10.1016/j.marpetgeo.2019.03.008.

Uncited references

Teichmüller, 1987; Tissot and Welte, 1984; Van Krevelen, 1984.

References

Batten D.J., Grenfell, H.R., 1996. Green and Blue-Green Algae. Palynology: Principles and Applications. 205–214.

Batten, D.J., Stead, D.T., 2005. Palynofacies analysis and its stratigraphic application. In: Applied Stratigraphy. Springer, Dordrecht, pp. 203–226.

Behar, F., Kressmann, S., Rudkiewicz, J.L., Vandenbroucke, M., 1992. Experimental simulation in a confined system and kinetic modelling of kerogen and oil cracking. Org. Geochem. 19 (1–3), 173–189.

Belcher, C.M., Mander, L., Rein, G., Jervis, F.X., Haworth, M., Hesselbo, S.P., Glaspool, I.J., McElwain, J.C., 2010. Increased fire activity at the Triassic/Jurassic boundary in Greenland due to climate-driven floral change. Nat. Geosci. 3 (6), 426.

Belka, Z., 1990. Thermal maturation and burial history from conodont colour alteration data, Holy Cross Mountains, Poland. Cour. Forschungsinstitut Senckenberg 118, 241–251.

Beyssac, O., Goffé, B., Chopin, C., Rouzaud, J., 2002. Raman spectra of carbonaceous material in metasediments: a new geothermometer. J. Metamorph. Geol. 20, 859–871.

Bonis, N.R., Kürschner, W.M., Krystyn, L., 2009. A detailed palynological study of the Triassic–Jurassic transition in key sections of the Eiberg basin (northern Calcareous Alps, Austria). Rev. Palaeobot. Palynol. 156 (3–4), 376–400.

Bonis, N.R., Ruhl, M., Kürschner, W.M., 2010. Climate change driven black shale deposition during the end-Triassic in the western Tethys. Palaeogeogr. Palaeoclimatol. Palaeoecol. 290 (1–4), 151–159.

Bonoldi, L., Frigerio, F., Di Paolo, L., Savoini, A., Barbieri, D., Grigo, D., 2018. Organic matter maturity profile of a well case study by Combination of Raman Spectroscopy and PCA-PLS Chemometric methods. Energy Fuel. 32 (9), 8955–8965.

Caricchi, C., Corrado, S., Di Paolo, L., Aldega, L., Grigo, D., 2016. Thermal maturity of Silurian deposits in the Baltic Syneclise (on-shore polish Baltic basin): contribution to unconventional resources assessment. Italian Journal of Geosciences 135 (3), 383–393.

Castiglioni, C., Tommasini, M., Zerbi, G., 2004. Raman spectroscopy of polyconjugated molecules and materials: confinement effect in one and two dimensions. Philosophical ransactions of the Royal Society of London. Series A: Mathematical, Physical and Engineering Sciences 362, 2425–2459.

Chen, Y., Mastalerz, M., Schimmelmann, A., 2012. Characterization of chemical functional groups in macerals across different coal ranks via micro-FTIR spectroscopy. Int. J. Coal Geol. 104, 22–33.

Cirilli, S., Marzoli, A., Tanner, L., Bertrand, H., Buratti, N., Jourdan, F., Bellieni, G., Kontak, D., Renne, P.R., 2009. Latest Triassic onset of the Central Atlantic magmatic province (CAMP) volcanism in the Fundy basin (Nova Scotia): new stratigraphic constraints. Earth Planet. Sci. Lett. 286 (3–4), 514–525.

Cirilli, S., Panfili, G., Buratti, N., Frixa, A., 2018. Paleoenvironmental reconstruction by means of palynofacies and lithofacies analyses: an example from the Upper Triassic subsurface succession of the Hyblean Plateau Petroleum System (SE Sicily, Italy). Rev. Palaeobot. Palynol. 253, 70–87.

Clayton, G., Goodhue, R., Abdelbagi, S.T., Vecoli, M., 2017. Correlation of Palynomorph Darkness Index and vitrinite reflectance in a submature Carboniferous well section in northern Saudi Arabia. Rev. Micropaleontol. 60, 411–416.

Collins, A., 1990. The 1–10 Spore Colour Index (SCI) scale: a universally applicable colour maturation scale, based on graded, picked palynomorphs. Meded. Rijks Geol. Dienst 45, 39–47.

Dadlez, R., 2001. Holy Cross Mts. area-crustal structure, geophysical data and general geology. Geol. Q. 45 (2), 99–106.

Dadlez, R., Kowalczewski, Z., Znosko, J., 1994. Some key problems of the pre- Permian tectonics of Poland. Geol. Q. 38 (2), 169–190.

Davies, J.H.F.L., Marzoli, A., Bertrand, H., Youbi, N., Ernesto, M., Schaltegger, U., 2017. End-Triassic mass extinction started by intrusive CAMP activity. Nat. Commun. 8, 15596.

Di Donato, E., Tommasini, M., Fustella, G., Brambilla, L., Castiglioni, C., Zerbi, G., Simpson, C.D., Müllen, K., Negri, F., 2004. Wavelength-dependent Raman activity of D2h symmetry polycyclic aromatic hydrocarbons in the D-band and acoustic phonon regions. Chem. Phys. 301, 81–93.

Espitalié, J., Marquis, F., Sage, L., 1987. Organic geochemistry of the Paris basin. Petroleum geology of North west Europe. Geological Society, London 1, 71–86.

Ferralis, N., Matys, E.D., Knoll, A.H., Hallmann, C., Summons, R.E., 2016. Rapid, direct and non-destructive assessment of fossil organic matter via microRaman spectroscopy. Carbon 108, 440–449.

Fisher, M.J., Barnard, P.C., Cooper, B.S., 1980. Organic maturation and hydrocarbon generation in the mesozoic sediments of the Sverdrup basin, Arctic Canada. In: Proceedings 4th International Palynological Conference, vol. 2, pp. 581–588.

Friedel, R., Carlson, G., 1972. Difficult carbonaceous materials and their infra-red and Raman spectra. Reassignments for coal spectra. Fuel 51, 194–198.

Ganz, H.H., Kalkreuth, W., Ganz, S.N., Öner, F., Pearson, M.J., Wehner, H., 1990. Infrared Analysis—State of the Art Berliner Geowissenshaftliche Abhandlungen, vols. 120–2, 1011–1026.

Goodhue, R., Clayton, G., 2010. Palynomorph Darkness Index (PDI) – a new technique for assessing thermal maturity. Palynology 34, 147–156.

Guedes, A., Valentim, B., Prieto, A.C., Rodrigues, S., Noronha, F., 2010. Micro-Raman spectroscopy of collotelinite, fusinite and macrinite. Int. J. Coal Geol. 83, 415–422.

Guedes, A., Valentim, B., Prieto, A., Noronha, F., 2012. Raman spectroscopy of coal macerals and fluidized bed char morphotypes. Fuel 97, 443–449.

Hackley, P.C., Lünsdorf, N.K., 2018. Application of Raman spectroscopy as thermal maturity probe in shale petroleum systems: insights from natural and artificial maturation series. Energy Fuel. 32 (11), 11190–11202.

Hakenberg, M., Świdrowska, J., 1997. Propagation of the south-eastern segment of the Polish Trough connected with bounding fault zones (from the Permian to the Late Jurassic). Comptes Rendus Acad. Sci. - Ser. IIA Earth Planet. Sci. 324 (10), 793–803.

Haseldonckx, P., 1979. Relation of palynomorph colour and sedimentary organic matter to thermal maturation and hydrocarbon generating potential. CCOP Techn. Bull. 6, 41–53.

Heusser, L.E., Stock, C.E., 1984. Preparation techniques for concentrating pollen from marine sediments and other sediments with low pollen density. Palynology 8 (1), 225–227.

Hillebrandt, A.V., Krystyn, L., Kürschner, W.M., Bonis, N.R., Ruhl, M., Richoz, S., Schobben, M.A.N., Urlichs, M., Bown, P.R., Kment, K., McRoberts, C.A., Simms, M., Tomãsových, A., 2013. The global stratotype sections and point (GSSP) for the base of the Jurassic system at Kuhjoch (Karwendel Mountains, northern Calcareous Alps, Tyrol, Austria). Episodes 36 (3), 162–198.

Hillier, S., Marshall, J.E.A., 1992. Organic maturation, thermal history and hydrocarbon generation in the Orcadian Basin. Scotland. J. Geol. Soc. 149, 491–502.

Hinrichs, R., Brown, M.T., Vasconcellos, M.A., Abrashev, M.V., Kalkreuth, W., 2014. Simple procedure for an estimation of the coal rank using micro-Raman spectroscopy. Int. J. Coal Geol. 136, 52–58.

Ibarra, J.V., Muñoz, E., Moliner, R., 1996. FTIR study of the evolution of coal structure during the coalification process organic. Geochemistry 24, 725–735.

Jubb, A.M., Botterell, P.J., Birdwell, J.E., Burruss, R.C., Hackley, P.C., Valentine, B.J., Hatcherian, J.J., Wilson, S.A., 2018. High microscale variability in Raman thermal maturity estimates from shale organic matter. Int. J. Coal Geol. 199, 1–9.

Kelemen S., Fang, H., 2001. Maturity trends in Raman spectra from kerogen and coal. Energy Fuel. 15, 653–658.

Konon, A., 2004. Successive episodes of normal faulting and fracturing resulting from progressive extension during the uplift of the Holy Cross Mountains, Poland. J. Struct. Geol. 26 (3), 419–433.

Konon, A., 2007. Strike-slip faulting in the Kielce unit, holy cross Mountains, central Poland. Acta Geol. Pol. 57, 415–441.

Kozłowski, W., Domanska-Siuda, J., Nawrocki, J., 2014. Geochemistry and petrology of the upper Silurian greywackes from the holy cross Mountains (central Poland): implications for the Caledonian history of the southern part of the trans-European suture zone (TESZ). Geol. Q. 58 (2), 311–336.

Kürschner, W.M., Herngreen, G.W., 2010. Triassic palynology of central and northwestern Europe: a review of palynofloral diversity patterns and biostratigraphic subdivisions. Geological Society, London, Special Publications 334 (1), 263–283.

Kutek, J., Głazek, J., 1972. The Holy Cross area, central Poland, in the alpine cycle. Acta Geol. Pol. 22 (4), 603–651.

Lahfid, A., Beyssac, O., Deville, E., Negro, F., Chopin, C., Goffé, B., 2010. Evolution of the Raman spectrum of carbonaceous material in low-grade metasediments of the Glarus Alps (Switzerland). Terra. Nova 22, 354–360.

Lamarche, J., Mansy, J., Bergerat, F., Averbuch, O., Hakenberg, M., Lewandowski, M., Stupnicka, E., Swidrowska, J., Wajsprych, B., Wieczorek, J., 1999. Variscan tectonics in the Holy Cross Mountains (Poland) and the role of structural inheritance during Alpine tectonics. Tectonophysics 313 (1–2), 171–186.

Legall, F.D., Barnes, C.R., Macqueen, R.W., 1981. Thermal maturation, burial history and hotspot development, Paleozoic strata of southern Ontario-Quebec, from conodont and acritarch colour alteration studies. Bull. Can. Petrol. Geol. 29, 492–539.

Li, C.-Z., 2007. Some recent advances in the understanding of the pyrolysis and gasification behaviour of Victorian brown coal. Fuel 86, 1664–1683.

Li, X., Hayashi, J.-I., Li, C.-Z., 2006. FT-Raman spectroscopic study of the evolution of char structure during the pyrolysis of a Victorian brown coal. Fuel 85, 1700–1707.

Lindström, S., van de Schootbrugge, B., Hansen, K.H., Pedersen, G.K., Alsen, P., Thibault, N., Dybkjær, K., Bjerrum, C.J., Nielsen, L.H., 2017. A new correlation of Triassic–Jurassic boundary successions in NW Europe, Nevada and Peru, and the Central Atlantic Magmatic Province: a time-line for the end-Triassic mass extinction. Palaeogeogr. Palaeoclimatol. Palaeoecol. 478, 80–102.

Lis, G.P., Mastalerz, M., Schimmelmann, A., Lewan, M.D., Stankiewicz, B.A., 2005. FTIR absorption indices for thermal maturity in comparison with vitrinite reflectance R 0 in type-II kerogens from Devonian black shales. Org. Geochem. 36, 1533–1552.

Liu, D., Xiao, X., Tian, H., Min, Y., Zhou, Q., Cheng, P., Shen, J., 2013. Sample maturation calculated using Raman spectroscopic parameters for solid organics: methodology and geological applications. Chin. Sci. Bull. 58, 1285–1298.

Lünsdorf, N.K., Lünsdorf, J.O., 2016. Evaluating Raman spectra of carbonaceous matter by automated, iterative curve-fitting. Int. J. Coal Geol. 160, 51–62.

Lünsdorf, N.K., Dunkl, I., Schmidt, B.C., Rantitsch, G., Von Eynatten, H., 2017. Towards a higher comparability of geothermometric data obtained by Raman spectroscopy of carbonaceous material. Part 2: a revised geothermometer. Geostand. Geoanal. Res. 41 (4), 593–612.

Lupoi, J.S., Fritz, L.P., Parris, T.M., Hackley, P.C., Solotky, L., Eble, C.F., Schlaegle, S., 2017. 323 assessment of thermal maturity trends in Devonian–Mississippian source rocks using Raman spectroscopy: limitations of peak-fitting method. Front. Energy Res. 5, 24.

Lupoi, J.S., Fritz, L.P., Hackley, P.C., Solotky, L., Weislogel, A., Schlaegle, S., 2018. Quantitative evaluation of vitrinite reflectance and atomic O/C in coal using Raman spectroscopy and multivariate analysis. Fuel 230, 1–8.

Marshall, J.E.A., Yule, B.L., 1999. Spore colour measurement. In: Jones, T.P., Rowe, N.P. (Eds.), Fossil Plants and Spores: Modern Techniques. Geological Society, London, pp. 165–168.

Marshall, C.P., Javaux, E.J., Knoll, A.H., Walter, M.R., 2005. Combined micro-Fourier transform infrared (FTIR) spectroscopy and micro-Raman spectroscopy of Proterozoic acritarchs: a new approach to palaeobiology. Precambrian Res. 138 (3–4), 208–224.

Martín-Closas, C., Permanyer, A., Vila, M.J., 2005. Palynofacies distribution in a lacustrine basin. Geobios 38, 197–210.

Marynowski, L., Simoneit, B.R., 2009. Widespread Upper Triassic to Lower Jurassic wildfire records from Poland: evidence from charcoal and pyrolytic polycyclic aromatic hydrocarbons. Palaios 24 (12), 785–798.

Mumm, A.S., Inan, S., 2016. Microscale organic maturity determination of graptolites using Raman spectroscopy. Int. J. Coal Geol. 162, 96–107.

Negri, F., Castiglioni, C., Tommasini, M., Zerbi, G., 2002. A computational study of the Raman spectra of large polycyclic aromatic hydrocarbons: toward molecularly defined subunits of graphite. J. Phys. Chem. A 106, 3306–3317.

Negri, F., di Donato, E., Tommasini, M., Castiglioni, C., Zerbi, G., Müllen, K., 2004. Resonance Raman contribution to the D band of carbon materials: modeling defects with quantum chemistry. J. Chem. Phys. 120, 11889–11900.

Pearson, D.L., 1990. Pollen/spore colour "standard". In: 2nd Printing of Version #2.

Pienkowski, G., 2004. The Epicontinental Lower Jurassic of Poland. vol. 12, Polish Geological Institute Special Papers, 1–154.

Pienkowski, G., Waksmundzka, M., 2009. Palynofacies in Lower Jurassic epicontinental deposits of Poland: tool to interpret sedimentary environments. Episodes 32 (1), 21–32.

Pieńkowski, G., Niedźwiedzki, G., Waksmundzka, M., 2012. Sedimentological, palynological and geochemical studies of the terrestrial Triassic–Jurassic boundary in northwestern Poland. Geol. Mag. 149 (2), 308–332.

Pimenta, M.A., Dresselhaus, G., Dresselhaus, M.S., Cancado, L.G., Jorio, A., Saito, R., 2007. Studying disorder in graphite-based systems by Raman spectroscopy. Phys. Chem. Chem. Phys. 9, 1276–1290.

Pócsik, I., Hundhausen, M., Koós, M., Ley, L., 1998. Origin of the D peak in the Raman spectrum of microcrystalline graphite. J. Non-Cryst. Solids 227, 1083–1086.

Potgieter-Vermaak, S., Maledi, N., Wagner, N., Van Heerden, J., Van Grieken, R., Potgieter, J., 2011. Raman spectroscopy for the analysis of coal: a review. J. Raman Spectrosc. 42, 123–129.

Quirico, E., Rouzaud, J.N., Bonal, L., Montagnac, G., 2005. Maturation grade of coals as revealed by Raman spectroscopy: progress and problems. Spectrochim. Acta Mol. Biomol. Spectrosc. 61, 2368–2377.

Rebelo, S.L., Guedes, A., Szefczyk, M.E., Pereira, A.M., Araújo, J.P., Freire, C., 2016. Progress in the Raman spectra analysis of covalently functionalized multiwalled carbon nanotubes: unraveling disorder in graphitic materials. Phys. Chem. Chem. Phys. 18, 12784–12796.

Reich, S., Thomsen, C., 2004. Raman spectroscopy of graphite. Phil. Trans. Roy. Soc. Lond.: Math. Phys. Eng. Sci. 362, 2271–2288.

Robl, T.L., Davis, B.H., 1993. Comparison of the HF-HCl and HF-BF 3 maceration techniques and the chemistry of resultant organic concentrates. Org. Geochem. 20, 249–255.

Ruhl, M., Kürschner, W.M., 2011. Multiple phases of carbon cycle disturbance from large igneous province formation at the Triassic-Jurassic transition. Geology 39 (5), 431–434.

Sadezky, A., Muckenhuber, H., Grothe, H., Niessner, R., Pöschl, U., 2005. Raman microspectroscopy of soot and related carbonaceous materials: spectral analysis and structural information. Carbon 43, 1731–1742.

Schaller, M.F., Wright, J.D., Kent, D.V., 2011. Atmospheric pCO2 perturbations associated with the Central Atlantic magmatic province. Science 331 (6023), 1404–1409.

Schito, A., Corrado, S., 2018. An automatic approach for characterization of the thermal maturity of dispersed organic matter Raman spectra at low diagenetic stages. Geological Society, London, Special Publications 484, SP484–S485.

Schito, A., Romano, C., Corrado, S., Grigo, D., Poe, B., 2017a. Diagenetic thermal evolution of organic 384 matter by Raman spectroscopy. Org. Geochem. 106, 57–67.

Schito, A., Corrado, S., Trolese, M., Aldega, L., Caricchi, C., Cirilli, S., Grigo, D., Guedes, A., Romano, C., Spina, A., Valentim, B., 2017b. Assessment of thermal evolution of paleozoic successions of the holy cross Mountains (Poland). Mar. Petrol. Geol. 80, 112–132.

Schito, A., Andreucci, B., Aldega, L., Corrado, S., Di Paolo, L., Zattin, M., Szaniawski, R., Jankowski, L., Mazzoli, S., 2018. Burial and exhumation of the western border of the Ukrainian Shield (Podolia): a multi-disciplinary approach. Basin Res. 30, 532–549.

Schmidt, J.S., Hinrichs, R., Araujo, C.V., 2017. Maturity estimation of phytoclasts in strew mounts by micro-Raman spectroscopy. Int. J. Coal Geol. 173, 1–8.

Schoene, B., Guex, J., Bartolini, A., Schaltegger, U., Blackburn, T.J., 2010. Correlating the end-Triassic mass extinction and flood basalt volcanism at the 100 ka level. Geology 38 (5), 387–390.

Sifeddine, a., Laggoun-Défarge, F., Lallier-Vergès, E., Disnar, J.R., Williamson, D., Gasse, F., Gibert, E., 1995. - La sédimentation organique lacustre en zone tropicale sud au cours des 36 000 dernières années (Lac Tritrivakely, Madagascar). Comptes Rendus de l'Académie des Sciences Paris, Series IIa 321, 385–391.

Smith, P.M.R., 1983. Spectral correlation of spore colouration standards. In: Brooks, J. (Ed.), Petroleum Geochemistry and Exploration of Europe. Geological Society, London, pp. 289–294.

Spina, A., Vecoli, M., Riboulleau, A., Clayton, G., Cirilli, S., Di Michele, A., Marcogiuseppe, A., Rettori, R., Sassi, P., Servais, T., Riquier, L., 2018. Application of Palynomorph Darkness Index (PDI) to assess the thermal maturity of palynomorphs: a case study from North Africa. Int. J. Coal Geol. 188, 64–78.

Staplin, F.L., 1969. Sedimentary organic matter, organic metamorphism and oil and gas occurrence. Bull. Can. Petrol. Geol. 17, 47–66.

Steffen, D., Gorin, G., 1993a. Palynofacies of the upper Tithonian-Berriasian deep-sea carbonates in the Vocontian trough (SE France). Bull. Cent. Rech. Explor.-Prod. Elf-Aquitaine 17, 235–247.

Steffen, D., Gorin, G.E., 1993b. Sedimentology of Organic Matter in Upper Tithonian-Berriasian Deep-Sea Carbonates of Southeast France: Evidence of Eustatic Control, (Chapter 5).

Szulczewski, M., Belka, Z., Skompski, S., 1996. The drowning of a carbonate platform: an example from the Devonian-Carboniferous of the southwestern Holy Cross Mountains, Poland. Sediment. Geol 106 (1), 21–49.

Taylor, G.H., Teichmüller, M., Davis, A.C.F.K., Diessel, C.F.K., Littke, R., Robert, P., 1998. Organic petrology: a new handbook incorporating some revised parts of Stach's textbook of coal petrology. Gebruder Borntraeger Verlagsb 704.

Teichmüller, M., 1987. Organic material and very low grade metamorphism. In: Frey, M. (Ed.), Low-temperature Metamorphism. Chapman & Hall, Glasgow, pp. 114–161.

Tissot, B.P., Welte, D.H., 1984. From kerogen to petroleum. In: Petroleum Formation and Occurrence. Springer, Berlin Heidelberg, pp. 160–198.

Traverse, A., 2007. What paleopalynology is and is not. In: Paleopalynology. Springer, Dordrecht, pp. 1–43.

Tuinstra, F., Koenig, J.L., 1970. Raman spectrum of graphite. J. Chem. Phys. 53, 1126–1130.

Tyson, R.V., 1995. Sedimentary Organic Matter — Organic Facies and Palynofacies Chapman and Hall, London, 1–615.

Van de Schootbrugge, B., Quan, T.M., Lindström, S., Püttmann, W., Heunisch, C., Pross, J., Fiebig, J., Petschick, R., Röhling, H.G., Richoz, S., Falkowski, P.G., Rosenthal, Y., 2009. Floral changes across the Triassic/Jurassic boundary linked to flood basalt volcanism. Nat. Geosci. 2 (8), 589.

Van der Zwan, C.J., 1990. Palynostratigraphy and palynofacies reconstruction of the upper Jurassic to lowermost Cretaceous of the Draugen field, offshore Mid Norway. Rev. Palaeobot. Palynol. 62 (1–2), 157–186.

Van Krevelen, D.W., 1984. Organic geochemistry—old and new. Org. Geochem. 6, 1–10.

Warren, J.K., 1986. Shallow-water evaporitic environments and their source rock potential. J. Sediment. Res. 56 (3), 442–454.

Whitaker, M., 1984. The usage of palynology in definition of Troll Field geology. In: Reduction of Uncertainties in Innovative Reservoir Geomodelling. 'Offshore' Northern Seas Conference, (No. 6).

Wilkins, R.W., Boudou, R., Sherwood, N., Xiao, X., 2014. Thermal maturity evaluation from inertinites by Raman spectroscopy: the 'RaMM' technique. Int. J. Coal Geol. 128, 143–152.

Wilkins, R.W., Sherwood, N., Li, Z., 2018. RaMM (Raman maturity method) study of samples used in an interlaboratory exercise on a standard test method for determination of vitrinite reflectance on dispersed organic matter in rocks. Mar. Petrol. Geol. 91, 236–250.

Williams, S.H., Burden, E.T., Mukhopadhyay, P.K., 1998. Thermal maturity and burial history of Paleozoic rocks in western Newfoundland. Can. J. Earth Sci. 35, 1307–1322.

Wood, G.D., Palmer-Koleman, S.E., Alemán, A.M., Padilla, H., 2002. Palynofacies and biomarker analysis of the lowermost permo–Carboniferous pular formation, a volcanic arc sequence in the Sierra de Almeida, northern Chile. Rev. Palaeobot. Palynol. 118 (1–4), 323–333.

Yule, B.L., Roberts, S., Marshall, J.E.A., 2000. The thermal evolution of sporopollenin. Org. Geochem. 31 (9), 859–870.